Research Square

Preprints are preliminary reports that have not undergone peer review.
They should not be considered conclusive, used to inform clinical practice,
or referenced by the media as validated information.

Interface-Engineered g-C_3 N_4 @CuAl-LDH Composite for Photocatalytic Degradation of Bromophenol Blue Dye

Ayesha Anwar
The Islamia University of Bahawalpur
Sami Ullah
Shanxi University
Muhammad Nadeem Akhtar
The Islamia University of Bahawalpur
Muhammad Akram
The Islamia University of Bahawalpur
Syed Shoaib Ahmad Shah
National University of Sciences and Technology
Muhammad Altaf Nazir
altaf.nazir@iub.edu.pk

The Islamia University of Bahawalpur

Research Article

Keywords: Graphite Carbon Nitride, Layered Double Hydroxide (LDH), g-C3N4@CuAl-LDH, water treatment, photocatalytic degradation, Bromophenol blue dye

Posted Date: March 14th, 2026

DOI: https://doi.org/10.21203/rs.3.rs-8860713/v1

License: This work is licensed under a Creative Commons Attribution 4.0 International License.
Read Full License

Additional Declarations: No competing interests reported.

Abstract

The development of effective environmental remediation materials is essential for solving the world's pollution problems. In this study g-C_3N_4@CuAl-LDH composite was synthesized for the photocatalytic removal of Bromophenol blue (BPB) dye from water. The enhanced surface area, active sites, and surface functional groups of the g-C_3N_4@CuAl-LDH composite lead to higher degradation capabilities for dye. The composites exhibit improved photocatalytic efficiency when exposed to visible light because of effective charge separation and transfer. The synthesized g-C_3N_4@CuAl-LDH composite was evaluated for the removal of BPB dye from water under various factors like pH and contact time of dye solutions. According to this study percentage degradation of g-C_3N_4@CuAl-LDH composite achieved to 83.37% after 60 minutes of contact time. Furthermore the value of correlation coefficient (R^2 =0.95757) suggested the first order kinetics with rate constant K_t (min^{-1}) = 0.02961. The g-C_3N_4@CuAl-LDH composite was found to be most active in photocatalysis under alkalinity with a BPB removal of 99.08% at pH 9. The most important reactive species regulating the breakdown of BPB, according to radical scavenging tests, are superoxide radicals ($O_2^{\cdot-}$); hydroxyl intermediates and holes produced in the presence of light are of second importance. Overall, this study serves as a foundation for the synthesis of advanced materials based on LDH for catalytic applications.

1. Introduction

In recent years, increasing attention has been directed toward the contamination of water bodies by organic dyes released from industries such as papermaking, textile dyeing, and related manufacturing sectors, due to their serious threat to human health [1]. Beyond their undesirable visual impact, discharged dyes can elevate aquatic toxicity and exhibit potential carcinogenic effects [2]. Moreover, many synthetic dyes are resistant to biodegradation and persist in the environment because of their complex molecular structures and xenobiotic nature. Consequently, the effective removal of color from dye-laden wastewater has become a critical environmental challenge. To address this issue, a variety of treatment technologies have been explored, including coagulation, biological processes, ion-exchange methods, membrane-based filtration, adsorption and photocatalytic degradation [3–5]. Photocatalytic degradation is an advanced and eco-friendly technique for removing pollutants from contaminated water. This process is particularly effective for persistent pollutants that are difficult to eliminate using conventional treatment methods. Owing to its low chemical consumption and potential use of sunlight as an energy source, photocatalysis is considered a sustainable approach for water purification [6].

Layered double hydroxides (LDHs) have grown to particular significant in recent years in context of photocatalysis [7]. The generic chemical formula $[M^{2+}_{1-x} M^{3+}_{x}(OH)_2]^{x+} (A^{n-})_{x/n}. mH_2O$ characterizes LDHs. The ions in the formula, M^{3+} and M^{2+}, can be replaced by trivalent and divalent cations respectively, while the interlayer anion is also allowed [8]. Since interlayer anions electronically balance the positively charged layers that constitute up LDHs, there is no net positive charge involved. Ion interactions with a range of distinct anionic molecules can therefore be used with this class of clays, in

contrast to cationic clays, which are often changed by organic ammonium ions [9]. They also have a high adsorption capacity and variable band gap, making them appropriate for cation-anion exchange [10]. Furthermore, the layered structure of LDH materials permits a wide range of crystal morphology, size, and form, in addition to the kinds of cations and anions that may be used to construct them. These features have a significant influence on charge transfer and separation efficiency, which in turn determines the total efficiency of photocatalytic reactions [11]. To further enhance their catalytic efficiency they can be coupled with other materials for improved performance.

The intriguing earth-abundant visible light photographic catalyst graphite carbon nitride (g-C_3N_4) has customizable electronic settings, unparalleled chemical stability, and a unique two dimensional structure. g-C_3N_4 is an ideal option to pair with different useful substances to improve performance because of its distinct electrical structure [12]. It is a graphene analog with layers that may change into various shapes, such as small quantum dots, nanosheets of material and nanostructures [13]. However, g-C_3N_4's photocatalytic activity is hampered by its comparatively small specified high rate and surface area of photogenerated pair of holes and electron recombination [14]. To overcome these limitations making composite with other materials is best known strategy. It has previously been seen that g-C_3N_4@LDH heterostructure are successful materials for degradation applications [15].

Jedras et al. reported silver modified LDH/GCN heterostructure with higher visible-light photocatalytic degradation of steroidal estrogens with more than 99% removal via improved charge separation and interfacial transfer of electrons [16], Lal et al. reported that CuCoFe-LDH/g-C_3N_4/$MoSe_2$ heterojunction demonstrated high degradation of bisphenol A (67% under solar and 53% under LED light) in a 6 hours' time period [17] similarly, Koduru et al. demonstrated that GCN/MgFe-LDH has a high remediation capacity and adsorption capacity of 312.30 mgg^{-1} for Cd(II) and 273.42 mgg^{-1} for U(VI), and over 5 reuse cycles [18]. Nevertheless, there has not been an investigation on the performance of the gC_3N_4@LDH composite with regard to removing Bromophenol Blue dye in water.

Herein, g-C_3N_4 and CuAl-LDH were combined and a g-C_3N_4@CuAl-LDH heterostructure was prepared by in situ hydrothermal approach for degradation of Bromophenol blue dye by photocatalytic processes. SEM, FTIR and XRD analyses proved the successful synthesis, the surface morphology and the structural characteristics of the composite. Systematic testing of photocatalytic performance was done by observing the impact of pH of the solution, contact time and starting concentration of dye. Lastly, the mechanism of photocatalytic degradation, and a comparison with the current literature were presented explaining the importance and efficiency of the g-C_3N_4-CuAl-LDH heterostructure.

2. Materials and Methods

2.1. Material

Urea (CH_4N_2O) (< 99%), Aluminum nitrate $Al(NO_3)_2$ (< 99%), Copper nitrate $Cu(NO_3)_2$ (< 99%), Bromophenol blue (98%) all of these compounds were acquired in analytical grade form Sigma Aldrich (Shanghai, P.R. China) and utilized without additional processing. The Islamia University of Bahawalpur, Pakistan's laboratory provided the distilled water.

2.2. Synthesis of g-C_3N_4

Urea powder was placed in a ceramic crucible and transferred to a preheated muffle furnace maintained at 550°C. The urea polymerized and decomposed thermally during the calcination process to release gaseous by-products. Once the heat treatment was over, the furnace was left to cool down to room temperature. The resultant product was a pale-yellow g-C_3N_4 (graphitic carbon nitrite) powder.

2.3. Synthesis of CuAl-LDH

Cu-Al-LDH was prepared by following the already reported method with some modifications [19]. Copper (II) and aluminum nitrate were dissolved in distilled water at a mass ratio of 2:1 (2g copper nitrate and 1g aluminum nitrate) using magnetic stirring for 10 minutes to form a homogenous solution. Separately, a 0.4 M solution of urea was obtained by mixing 2.4 g of urea and 100 mL of distilled water under continuous stirring. Slowly the urea solution was added to the metal nitrate solution under constant stirring. After refluxing the mixture for 48 hours, a blue precipitate was produced. After allowing the reaction to continue, the suspension was centrifuged for 10 minutes at 6000 rpm to extract the solid product. CuAl-LDH powder was obtained by completely washing the product with distilled water, drying it in an oven, and grinding it.

2.4. Synthesis of g-C_3N_4@CuAl-LDH Composite

Nickel nitrate and aluminum nitrate were dissolved in distilled water in a 2:1 ratio of mass (2 g and 1 g, respectively) to form a homogeneous solution after 20 min of magnetic stirring. Separately, a 0.4 M solution of urea was obtained by mixing 2.4 g of urea and 100 mL of distilled water under continuous stirring. Slowly the urea solution was added to the metal nitrate solution under constant stirring. Then, 0.1g of the graphitic carbon nitride (g-C_3N_4) was added in pre-synthesized form and the mixture stirred, allowing the dispersion of the particles to be even. A mixture of the reactants was under heating and stirring (48 h) to form a green-colored compound. The product was washed, centrifuged, dried at 100°C in oven, and ground in a fine powder to obtain g-C_3N_4@CuAl-LDH composite **(**Fig. 1**).**

2.5. Photocatalytic Degradation Experiment

To investigate the photocatalytic properties of the as-prepared g-C_3N_4@CuAl-LDH composite, the dye degradation of Bromophenol blue (BPB) was considered under various experimental conditions without light and under light irradiation of the visible light. The individual components and the composite were studied concerning the photocatalytic activities in the presence of BPB as a model organic pollutant at

acidic and basic PH conditions. The highest absorption wavelength (λ max) of the Bromophenol blue was noted at about 590 nm.

Electrons in the photocatalyst were excited upon visible light irradiation between the valence bands to the conduction band to form electron-hole (e^-/h^+) pairs. These charge carriers were involved in redox reactions thereby degrading BPB dye molecules. To determine the efficacy of the photocatalytic degradation, it was computed using Eq. (1):

Degradation efficiency (%) = $(C_o - C_t / C_o) \times 100$ (1)

Where C_o and C_t are the dye initial concentration and the concentration at time t, respectively

The photoluminescence (PL) emission spectroscopy has been used to evaluate the charge carrier recombination behavior because the radiation sources of the photoluminescence emission are the radiant recombination of photoinduced electrons and holes [20]. The generally anticipated relationship between the higher and lower PL intensity is that, higher PL intensity is related to rapid recombination and the lower intensity indicates effective charge separation. The bare materials had comparatively greater PL emission, which implies a quicker recombination of electrons and holes. Contrastingly, the g-C_3N_4@CuAl-LDH composite had much lower PL intensity, meaning that it inhibited the recombination of photogenerated charge carriers. Such a decrease promotes charge separation efficiency and increases the lifespan of the active species, which improves the overall performance of photocatalysis of the composite material.

2.6. Characterization Techniques

Fourier transform infrared (FTIR) spectroscopy was used to analyze functional groups of g-C_3N_4, CuAl-LDH and their composite using an Agilent Cary instrument. The absorption of light of the synthesized materials was measured by UV-visible spectroscopy with Jenway 7135 spectrophotometer. The phase composition and crystallinity were obtained through X-ray diffraction (XRD) analysis using Shimadzu XRD-6000 system using λCu -Kα = 1.5406. The morphological characteristics of the samples prepared were analyzed with field-emission scanning electron microscopy (FESEM, JSM-7800, and Japan).

3. Results and discussion

3.1. Characterization

The surface morphologies of g-C_3N_4, CuAl-LDH, and g-C_3N_4@CuAl-LDH composite were examined using scanning electron microscopy (SEM). The SEM images reveal that pristine g-C_3N_4 displays a layered, sheet-like structure consisting of thin, uneven nanosheets with a wrinkled and folded shape. The thermally condensed g-C_3N_4 structure, which is constructed using nitrogen-rich precursors, has hollows between these loosely stacked sheets that provide interlayer gaps and porous networks. Because of its porosity and surface area, which have been shown to facilitate surface reactions, charge separation, and

mass transport, g-C_3N_4 is ideally suited for catalytic application (Fig. 2a) [21]. The CuAl-LDH has the near floral shape, which is owing to the huge number of erratically and randomly oriented nanosheets that build layered structures with effective dispersion of crystals. These are interconnected, flexible nanoplates that wrap around one another to produce interlocking balls made of layers that are aligned correctly. The CuAl-LDH sample also exhibits a large concentration of interconnected macropores that arise between the layers, which allows the hierarchical porous structure to be produced (Fig. 2b) [22]. In the case of the g-C_3N_4@CuAl-LDH composite the SEM image shows a unique morphology of the composite when compared to that of the pristine components. The composite has a coarse and agglomerated surface structure, with the CuAl-LDH particles uniformly anchored on, as well as spread across the g-C_3N_4 sheets. The initial layered structure of g-C_3N_4 is diminished because of thick overlay of LDH nanostructures, which results in the development of compact granular aggregates. This close interfacial interaction between g-C_3N_4 and CuAl-LDH implies effective composite formation and is likely to promote effective charge transfer and synergistic interactions, which will help to improve catalytic and photocatalytic activity (Fig. 2c-d).

The FTIR of g-C_3N_4 has characteristic absorption bands that confirm the successful synthesis of the material (Fig. 3a). The peak of 833 cm^{-1} is explained by the out-of-plane bending vibration of triazine/heptazine rings, and the band at 1062 cm^{-1} is explained by the ring-breathing modes. An absorption at 1149 and 1353 cm^{-1} is due to aromatic C-N stretching. Strong band 1638 cm^{-1} is related to C = N stretching of heptazine. The band at 1785 cm^{-1} is attributed to C = O stretching, which is a surface oxidation or defect sites. The absorption at 2422 cm^{-1} is attributed to adsorb CO_2 whereas the band at 2156 cm^{-1} is attributed to C ≡ N stretching. Lastly, the wide band at 3289 cm^{-1} is attributed to N-H stretching with O-H contributions of adsorbed water [23, 24]. The FTIR spectrum of pure Cu-Al-LDH shows specific absorption bands which prove the formation of the structure of layers of the double hydroxide (Fig. 3b). At 801 cm^{-1}, the band has been assigned to the lattice vibration modes of M-O and O-M-O bonds (M = Cu, Al) [25]. The peak at 963 cm^{-1} is attributed to metal-hydroxyl vibrations and the absorption at 1077 cm^{-1} is attributed to interlayer carbonate vibrations in the stretching mode [26]. The appearance of the band at 1353 cm^{-1} also supports the existence of carbonate anions. The highest frequency at 1638 cm^{-1} is caused by the bending water molecules in between the layers. The weak absorption between 2156 cm^{-1} is correlated with combination of carbonate modes. Lastly, the O-H stretching vibrations of the hydroxyl groups of the brucite-like layers and hydrogen-bonded interlayer water are observed to cause the broad band at 3373 cm^{-1} [22]. The FTIR spectrum of the g-C_3N_4@Cu-Al-LDH composite (Fig. 3c) has absorption bands associated with the g-C_3N_4 and the Cu-Al-LDH, suggesting that a successful formation of the composite took place. The band at 827 cm^{-1} is due to the out-of-plane bending vibration of triazine/heptazine rings and the 1077 cm^{-1} band is due to interlayer carbonate stretching vibrations of the LDH phase [26]. The aromatic C-N stretching vibrations give a peak at 1339 cm^{-1} and the C = N stretching of g-C_3N_4 and surface C = O groups give a peak at 1653 and 1733 cm^{-1}, respectively. The adsorbed carbonate related combination modes are associated with the

weak band at 2156 cm^{-1}. Lastly, O-H and N-H stretching vibrations of hydroxyl layers, interlayer water, and g-C_3N_4 have a broad band at 3358 cm^{-1}, which implies that the two components interact strongly at the interface [22–24].

The XRD pattern of g-C_3N_4 has a weak diffraction at 2θ ≈ 10.67° indexed to the (100) plane, which is the in-plane tri-s-triazine (heptazine) unit structural ordering. This peak confirms a periodic structure of the conjugated aromatic structure. The highest diffraction peak is at 2θ ≈ 27.80°, the typical interplanar stacking peak of graphitic carbon nitride and corresponds to (002) plane of graphitic materials (JCPDS No. 87-1526). This little variation of the peak with the standard value can be ascribed to small variations in interlayer spacing, probably due to structural distortion or defect formation, though it still proves the existence of well-defined layered g-C_3N_4 structure **(**Fig. 4a**)** [27]. The XRD pattern of CuAl-LDH has specific peak of diffraction at 2θ ≈ 31.7°, 34.3°, and 36.18°, indicating the (012), (015) and (018), respectively, which is formed due to the ordered arrangement of the Cu-Al brucite-like hydroxide layers. Such peaks represent high crystallinity and even distribution of cations in the LDH structure. The reflection at 47.5° indexed to the (110) plane is associated with in-plane metal-oxygen bonding, which implies a platelet or nanosheet-like structure. The increased angle 56.54° (116), 62.8° (018), and 67.8° (300) correspond to long-range lattice ordering and crystallites growth **(**Fig. 4b**)** [28, 29]. The XRD result of the g-C_3N_4@CuAl-LDH composite confirms that the heterostructured material formation with preserved phases of both the components was successful **(**Fig. 4c**).** Its (002) diffraction peak at 2θ ≈ 27.86° is retained which proves that the graphitic layered framework is still present with decreased strength because of the strong interfacial interaction with LDH layers. Moreover, the characteristic CuAl-LDH diffraction peaks at 30.44°, 33.43°, 35.65°, 41.31°, 52.50°, and 59.16° can be indexed to the (006), (012), (015), (018), (110), and (113) planes, respectively, which appear slightly broadened. This tendency implies the decreased crystallite size, partially exfoliation-based, and close interfacial interactions between sheets of g-C_3N_4 and CuAl-LDH nanosheets, with no precipitation of impurity phases [16, 30].

3.2. Photocatalytic Degradation of BPB

Photodegradation is the recalcitrant breakdown of organic pollutants into less toxic substances by the reactive species, including but not limited to: holes, peroxide radicals, and superoxide radicals, also referred to as reactive oxygen species (ROS). These ROS are primarily produced in a suspension with a catalyst and dye on the exposure to the appropriate light or activating agent. These are a few aspects that affect the effectiveness of the dye photodegradation considerably. Some of these major factors are discussed in the next section of this manuscript.

3.2.1. Effect of pH

One of the parameters that are used to measure photocatalytic performance of the synthesized materials is pH of the solution, since it directly relates to surface charge properties, dye speciation, and the formation of reactive oxygen species. In order to study this effect, batch photodegradation was

performed by using BPB dye at an initial concentration of 20ppm under acidic (pH 3) and alkaline (pH 9) conditions. All experiments were done under the same conditions of reactions and the pH of the BPB solutions adjusted and maintained with 1 M NaOH and HCl.

Under acidic conditions, all materials were inefficient at degrading (Fig. 5a), with g-C_3N_4 showing the lowest degradation rate of 9.43% for BPB, indicating weak surface reactions at an excess concentration of H^+ ions. CuAl-LDH was slightly more active with 16.24% degradation and this can be explained with moderate surface interaction of the dye molecules. The composite showed much better ability to perform than the pristine components with results of 36.31% degradation. Under basic conditions, which enhance effective charge separation and surface redox reactions, alkaline conditions exhibited a significant increase in the efficiency of photodegradation (Fig. 5b). g-C_3N4 was more effective in catalyzing photodegradation (28.33% degradation) because it is more stable and can also catalyze redox reactions on surfaces [31, 32]. CuAl-LDH displayed a significant growth in efficiency with degradation of 51.59% that can be explained by the increased accessibility of OH^- ions to hydroxyl radicals formation [33]. Markedly, the composite showed excellent photocatalytic activity with a degradation of BPB of 99.08% which corresponds to almost the entire elimination of the dye.

The increase in activity at pH 9 is mainly explained by the predominant action of OH^- ions in the formation of highly reactive hydroxyl radicals, and the abundance of the H^+ ions in acidic media inhibit photocatalytic activity. These results establish that alkaline pH is the most effective in BPB degradation especially when the composite material is used.

3.2.2. Impact of time contact

The impact of the irradiation time on photocatalytic degradation of BPB was researched by batch experiments in normal pH with an initial dye concentration of 20 ppm. Figure 6a-d compared the photocatalytic performance of g-C_3N_4, LDH and the composite at irradiation time of 0, 20, 40, and 60 min.

In the case of g-C_3N_4, the rate of BPB degradation was slow with time, which ranged at 13.97%, 22.40%, and 25.23% at 20, 40 and 60 min, respectively, which shows that the photocatalytic activity was limited. The degradation of CuAl-LDH showed stronger time-dependent increase (19.59%, 47.47% and 73.86%) degradation in the identical time periods, as a result of increased surface reactivity and with progressive radical generation. Conversely, the composite exhibited the greatest degradation degree whereby the faster removal of the BPB was observed over time with increasing irradiation time. The efficiencies of 39.90%, 78.23%, and 83.37% at 20, 40, and 60 min, respectively, indicated good efficiencies in charge separation and high synergistic interactions between g-C_3N_4 and CuAl-LDH.

It is known that the efficiency of degradation rises directly in relation to the longer the operational (irradiation) time, where longer contact between the dye and the catalyst enhances the interaction between the catalyst and the dye and continuous formation of the reactive species [34]. The study at

hand explains the observation that the extent of BPB degradation increasing with the time of irradiation of all the catalysts can be explained by the sustained generation and accumulation of reactive oxygen species, enhanced accessibility to active sites, and longer interactions between BPB molecules and the catalyst surface. Consequently, there is an incremental increase in the rate of degradation, and the composite catalyst has a better performance in batch mode at normal pH. Nonetheless, the degradation rate would decrease with longer irradiation times, because of depletion of dyes, recombination of electrons and holes and the possible accumulation of intermediate byproducts [35]. This means that the longer the duration of contact, the greater the break-down of the BPB, but the greater the exposure the weaker the impact and the composite catalyst was the most efficient under batch conditions with normal pH.

3.3. Kinetics Studies

The photocatalytic degradation reaction of the catalysts obtained could be classified according to the Langmuir-Hinshelwood kinetic model that is typically used to treat heterogeneous photocatalytic photoreactions. At certain concentrations of dye, the model can be reduced to a pseudo-first-order expression of the kinetics, which is presented in Equations (2) and (3) [36]:

$dC/dt = - K_1c$ (2)

$\ln (C_t/C_0) = k_1t$ (3)

In which C_0, C_t are the starting BPB concentration and the concentration at the time of irradiation, respectively, and k (min^{-1}) is the apparent pseudo first order rate constant. The slope of the linear graph of $-\ln(C_t/C_0)$ vs irradiation time t is used to determine the value of k, which is a measure of the photocatalytic degradation efficiency of BPB using each catalyst.

Among the investigated photocatalysts, g-C_3N_4 showed slowest kinetic rate constant K_t = 0.00548 min^{-1}), which could be explained by inefficient charge separation and lower surface reactivity. The rate constant (k_t = 0.0183 min^{-1}) of CuAl-LDH was much higher, which is an indication of the increased photocatalytic activity of this material because of the improved surface interactions and formation of reactive oxygen species. It is noteworthy that the g-C_3N_4@CuAl-LDH composite had the highest kinetic rate constant (k_t = 0.02961 min^{-1}) that proved its high photocatalytic activity in the degradation of BPB. The improved kinetics of the composite can be explained by synergies between g-C_3N_4 and CuAl-LDH, which facilitate the efficient separation of charges, inhibit the electron-hole recombination and enhance fast interfaces charge transfer.

The large linear regression coefficients (R_2 >0.95) of g-C_3N_4@CuAl-LDH heterostructure confirm that the experimental data is well represented by the pseudo-first-order kinetic model and Langmuir-Hinshelwood mechanism can be used in the case of BPB photodegradation in the conditions examined **(**Fig. 7a-b**).** According to the Langmuir-Hinshelwood kinetic analysis, the apparent pseudo-first-order rate constants

(k_t) and the resulting correlation coefficients (R^2) of the BPB degradation in the presence of the synthesized catalysts are shown in Table 1.

Table 1
The kinetics data for the photocatalytic degradation of BPB dye using as synthesized catalyst

Dye	**Catalyst**	**Langmuir model** K_t **(min^{-1})**	R^2
Bromophenol blue	g-C_3N_4	0.00548	0.94987
	CuAl-LDH	0.0183	0.89006
	g-C_3N_4@CuAl-LDH	0.02961	0.95757

3.4. Degradation Mechanism

The overall process that determines photocatalytic degradation of BPB though the g-C_3N_4@CuAl-LDH composite is the electronic interaction between the two semiconducting materials and efficiency of interfacial charge transfer. The values of band-gaps used in the presented mechanism are founded on the existing research by earlier researchers, in which g-C_3N_4 has a band gap of 2.7 eV and CuAl-LDH has a broader band gap of 3.4 eV [30]. Such difference in band-gap energy is vital in making the separation of photogenerated charge carriers easy, and highly discouraging electron-hole recombination.

When g-C_3N_4 and CuAl-LDH are irradiated by light they are both photo excited and produce electrons and holes respectively in the conduction and valence bands respectively. Due to the positive alignment of their band-edge potential, photogenerated electrons selectively enter the conduction band of CuAl-LDH to the conduction band of g-C_3N_4 and holes are excited onto the CuAl-LDH constituent. This directional flow of charge carriers increases their lifetime, increases interfacial charge separation, and finally facilitates photocatalytic activity.

The electrons that are photogenerated on the surface of g-C_3N_4 engage into the reduction reaction with dissolved molecular oxygen that generates superoxide radicals ($O_2.^-$). The radical trapping experiments support the predominant role of these radicals in the process of BPB degradation by demonstrating that a great part of photocatalytic activity is inhibited when superoxide scavengers are added. Simultaneously, holes produced by photo-generation process play a role in oxidation either directly or indirectly by the reaction of hydroxyl radicals (OH) with surface-adsorbed water molecules or hydroxide ions as further corroborated by the respective scavenger product. These reactive oxygen species are highly reactive that trigger a series of oxidative reactions that degrade BPB molecules into intermediate products, which are eventually decomposed to end products that have no adverse effects on the environment, including CO_2 and H_2O as shown in Fig. 8 and the subsequent equations (Eq. 3–6).

Reaction Equations:

$g\text{-}C_3N_4@CuAl\text{-}LDH + hv \rightarrow e^- + h^+$ (3)

$e^- + O_2 \rightarrow O_2^{\bullet -}$ (4)

$h^+ + H_2O/OH^- \rightarrow \bullet OH$ (5)

$BPB + O_2^{\bullet -}/\bullet OH/h^+ \rightarrow CO_2 + H_2O$ (6)

3.5. Reusability

To determine the stability and reusability of the $g\text{-}C_3N_4@CuAl\text{-}LDH$ composite to be used in repeated photocatalytic reactions, the reusability of this composite was studied. Following every photocatalytic cycle, the used catalyst was removed with a lot of care out of the reaction mixture and hot distilled water and ethanol were added to it in order to wash the catalyst product free of any adsorbed dye molecules or reaction intermediates. The catalyst recovered was dried at 80 ^{O}C over a period of 24 h and used again in the next cycle. Four repeats of this procedure were carried out keeping the same experimental conditions.

The efficiency of BPB degradation was gradual as indicated in Fig. 9a with an increase in the number of cycles. The first degradation rate of 83.37% in the first cycle reduced slightly by 80%, 76%, and 70% in the second, third, and fourth cycles respectively. The loss of photocatalytic activity observed could be related to the loss of catalyst during the recovery, the partial occupation of the active sites by the intermediate reaction products or the slight deactivation of the surfaces under high-long irradiation.

Although this was observed to decrease, the composite still retained a considerable percentage of its photocatalytic activity even in the fourth consecutive cycle, which indicated good structural stability and photo corrosion resistance. The comparatively low loss of activity shows that the $g\text{-}C_3N_4@CuAl\text{-}LDH$ composite is reusable satisfactorily, which indicates that it can be used in the photocatalytic treatment of wastewater within a long, duration of time. Comparison of the % degradation of various photocatalysts for the removal of BPB dye is given in Table 2.

Table 2
Comparison of the % degradation of various photocatalysts for the removal of BPB dye

Photocatalyst	Irradiation Source	Degradation Efficiency (%)	Time (min)	Ref.
$MgFe_2O_4$@CuO	Sunlight	90.94%	45 min	[37]
Gr/Cts NCs	Visible light	95.3%	240 min	[38]
Bi_2S_3@MIL-100	Sunlight	97%	80 min	[39]
$CuFe_2O_4$	Sunlight	93.6%	120 min	[40]
GR/β-CD	Sunlight	100%	120 min	[41]
TiO_2/GNP	UV light	86%	8 h	[42]
TiO_2 nanocomposites	UV lamp (55 Watts)	98%	20 min	[43]
ZnO	UV light (Xe arc lamp 20 W)	65%	150 min	[44]
Cu-doped ZnO	UV light (Xe arc lamp 20 W)	87%	150 min	[44]
γ-irradiated $MgFe_2O_4$ (4.5kGy)	Solar light	82.75%	140 min	[45]
γ-irradiated $MgFe_2O_4$ (3kGy)	Solar light	63.07%	140 min	[45]
g-C_3N_4@CuAl-LDH	**Sunlight**	**83.37%**	**60 min**	**This work**

3.6. Radical Trapping (Scavenging) Experiments

To determine the most active reactive species in the photocatalytic degradation of BPB the radical trapping experiments were conducted on the g-C_3N_4@CuAl-LDH composite. Isopropanol (IPA) was an example of a hydroxyl radical (-OH) scavenger, DMSO was an electron (e^-) scavenger, citric acid (CA) was a hole (h^+) scavenger, and benzoquinone (BPQ) was a superoxide radical ($O_2.^-$). The degradation efficiencies that were obtained with the presence of the scavengers were compared to the blank study.

The photocatalytic system in the absence of any scavenger had a degradation efficiency of BPB of 83.37%. When IPA was added, the degradation efficiency was reduced to 63%, which shows the presence of hydroxyl radical in the degradation process. When the use of DMSO was added, the efficiency reduced even more to 58% implying that photo generated electrons are important in terms of triggering reduction reactions that result in the formation of reactive species. With CA present, the degradation rate was halfed which proved that photogenerated holes contributed to oxidation of BPB. The greatest inhibition was also recorded in the presence of BPQ where the degradation efficiency decreased abruptly to 21%.

This drastic reduction is a clear indication that the most predominant reactive species that causes BPB degradation is the superoxide radicals ($O_2.^-$), which is produced during the interactions of electrons and oxygen.

All in all, the scavenging data indicates that the radical-mediated process of photocatalytic BPB degradation is mainly predominated by $O_2.^-$ radicals since the electrons, hydroxyl radicals and the photogenerated holes are secondary factors **(**Fig. 9b**).** These results are quite firm in the proposed degradation of the g-C_3N_4@CuAl-LDH composite through charge-transfer and band-gap-driven degradation mechanism.

Conclusion

The synthesized g-C_3N_4@CuAl-LDH composite was examined in this study in relation to the photocatalytic degradation of Bromophenol blue (BPB) in aqueous solution. The composite showed much better photocatalytic behavior than bare g-C_3N_4 and CuAl-LDH that is primarily due to efficient interfacial charge and repressed electron-holes recombination because of good band-gap coupling. Solution pH greatly influenced the degradation efficiency as the maximum BPB removal (99.08%) occurred in the cases of alkaline (pH 9) conditions. Time dependent tests indicated that the composite degraded 83.37% of BPB in 60 min of contact time. Kinetic analysis showed that the degradation reaction is pseudo-first-order since the correlation coefficient (R^2 = 0.95757) is high and the apparent rate of the degradation reaction is k_t = 0.02961 min^{-1}. The radical trapping experiments found the superoxide radicals ($O_2.^-$) as the most crucial reactive species, and the hydroxyl radicals and holes caused by the photo generation were secondary factors. In addition, the composite was highly stable and reused during different cycles. On the whole, these findings demonstrate that g-C_3N_4@CuAl-LDH compound is a potential, efficient, and stable photocatalyst that can be used in the treatment of wastewater.

Declarations

Declaration of competing interest

The authors declare that they have no known competing financial interests or personal relationships that could have appeared to influence the work reported in this paper.

Funding statement:

None

Author Contribution

CRediT authorship contribution statementAyesha Anwar: Writing – original draft, Methodology, Investigation, Data curation. Sami Ullah: Writing – review & editing, Formal analysis, Data curation. Muhammad Nadeem Akhtar: Software, Resources, Formal analysis. Muhammad Akram: Writing – review & editing, Visualization, Validation. Syed Shoaib Ahmad Shah: Syed Shoaib Ahmad Shah: Writing – review & editing, Supervision, Software, Resources. Muhammad Altaf Nazir: Writing – review & editing, Supervision, Project administration, Funding acquisition, Conceptualization.

Acknowledgements

The Authors are appreciated the Isntitute of Chemistry, The Islamia University of Bahawalpur (IUB), Pakistan for facilitating us by ensuring the necessary provisions to complete this research work.

References

1. Nazir MA et al (2022) Heterointerface engineering of water stable ZIF-8@ZIF-67: Adsorption of rhodamine B from water. Surf Interfaces 34:102324
2. Nazir MA et al (2024) Copper- and Manganese-Based Bimetallic Layered Double Hydroxides for Catalytic Reduction of Methylene Blue. Catalysts 14(7):430
3. Afzal S et al (2025) Synergistic Effect SnO2/g-C3N4 Heterojunction Cocatalyst for Photodegradation of Methyl Orange. ChemistrySelect 10(23):e02037
4. Nazir MA et al (2025) Zeolitic imidazolate frameworks (ZIF-8 & ZIF-67): Synthesis and application for wastewater treatment. Sep Purif Technol 356:129828
5. Ullah S et al Synthesis of MIL-88@activated carbon composite as an efficient adsorbent for the removal of Rhodamine B. Int J Environ Anal Chem : p. 1–19
6. Bekele T, Alamnie G (2025) The photocatalytic degradation of organic pollutants-a comprehensive overview. Results Chem 18:102758
7. Liu Z et al (2024) Light-driven C1 Chemical Conversion with LDH-based Nanomaterials. Appl Clay Sci 258:107488
8. Riaz S et al (2024) Recent advancement in synthesis and applications of layered double hydroxides (LDHs) composites. Mater Today Sustain 27:100897
9. Costa FR et al (2008) Intercalation of Mg–Al layered double hydroxide by anionic surfactants: preparation and characterization. Appl Clay Sci 38(3–4):153–164
10. Yan K, Wu G, Jin W (2016) Recent advances in the synthesis of layered, double-hydroxide-Based materials and their applications in hydrogen and oxygen evolution. Energy Technol 4(3):354–368
11. Nishimura S, Takagaki A, Ebitani K (2013) Characterization, synthesis and catalysis of hydrotalcite-related materials for highly efficient materials transformations. Green Chem 15(8):2026–2042
12. Zhao Z, Sun Y, Dong F (2015) Graphitic carbon nitride based nanocomposites: a review. Nanoscale 7(1):15–37

13. Rono N et al (2021) A review of the current status of graphitic carbon nitride. Crit Rev Solid State Mater Sci 46(3):189–217
14. Ong W-J et al (2016) Graphitic Carbon Nitride (g-C3N4)-Based Photocatalysts for Artificial Photosynthesis and Environmental Remediation: Are We a Step Closer To Achieving Sustainability? Chem Rev 116(12):7159–7329
15. Jędras A et al (2024) Tuning the Structural and Electronic Properties of Zn–Cr LDH/GCN Heterostructure for Enhanced Photodegradation of Estrone in UV and Visible Light. Langmuir 40(34):18163–18175
16. Jędras A et al (2025) Silver modified LDH/GCN heterostructures for visible-light degradation of estrogens, vol 15. Catalysis Science & Technology, pp 6792–6804. 22
17. Lal AS, Mishra NS, Saravanan P (2026) Synergistic charge transfer promoted staggered heterojunction built CuCoFe-LDH/g-C3N4/MoSe2 with enriched generation of superoxide radical for solar and LED photocatalysis. J Alloys Compd 1053:186225
18. Koduru JR et al (2024) Enhancing Cd(II) and U(VI) remediation through synergistic utilization of GCN-supported MgFe-layered double hydroxide. J Water Process Eng 57:104610
19. Boumeriame H et al (2023) Engineering g-C3N4 with CuAl-layered double hydroxide in 2D/2D heterostructures for visible-light water splitting. J Colloid Interface Sci 652:2147–2158
20. Riaz S et al (2025) Synthesis of CuFe-LDH/MIL-88 Composite for the Photocatalytic Degradation of Methyl Orange Dye. ChemistrySelect 10(17):e202500858
21. Al Mais D et al (2024) *Various Morphologies of Graphitic Carbon Nitride (g-C3N4) and Their Effect on the Thermomechanical Properties of Thermoset Epoxy Resin Composites.* Polymers, 16(13): p. 1935
22. Li J et al (2017) A novel three-dimensional hierarchical CuAl layered double hydroxide with excellent catalytic activity for degradation of methyl orange. RSC Adv 7(46):29051–29057
23. Fahimirad B, Asghari A, Rajabi M (2017) Magnetic graphitic carbon nitride nanoparticles covalently modified with an ethylenediamine for dispersive solid-phase extraction of lead(II) and cadmium(II) prior to their quantitation by FAAS. Microchim Acta 184(8):3027–3035
24. Sunasee S et al (2019) Sonophotocatalytic degradation of bisphenol A and its intermediates with graphitic carbon nitride. Environ Sci Pollut Res 26(2):1082–1093
25. Wu L et al (2019) Atomic layer deposition-assisted growth of CuAl LDH on carbon fiber as a peroxidase mimic for colorimetric determination of H 2 O 2 and glucose. New J Chem 43(15):5826–5832
26. Peng X et al (2018) Multipath fabrication of hierarchical CuAl layered double hydroxide/carbon fiber composites for the degradation of ammonia nitrogen. J Environ Manage 220:173–182
27. Das D et al (2018) Low temperature synthesis of graphitic carbon nitride nanorods for heavy metal ions sensing. Solid State Sci 82:99–105
28. Wu S et al (2023) A co-precipitation route for the preparation of eco-friendly Cu-Al-layered double hydroxides with efficient tetracycline degradation. Environ Sci Pollut Res 30(44):99412–99426

29. Kim W et al (2017) Methanol-steam reforming reaction over Cu-Al-based catalysts derived from layered double hydroxides. Int J Hydrog Energy 42(4):2081–2087
30. Rath A et al (2025) A novel Cu–Al LDH/g-C3N4 Z-scheme photocatalyst for environmental remediation of cresol red. Discover Appl Sci 7(8):846
31. Ahmed MA, Mahmoud SA, Mohamed AA (2024) Unveiling the photocatalytic potential of graphitic carbon nitride (gC 3 N 4): a state-of-the-art review. RSC Adv 14(35):25629–25662
32. Afzal S et al (2025) Synergistic Effect SnO2/g-C3N4 Heterojunction Cocatalyst for Photodegradation of Methyl Orange. ChemistrySelect 10(23):e02037
33. Nazir MA et al (2024) Copper-and manganese-based bimetallic layered double hydroxides for catalytic reduction of methylene blue. Catalysts 14(7):430
34. Anju Chanu L et al (2019) Effect of operational parameters on the photocatalytic degradation of Methylene blue dye solution using manganese doped ZnO nanoparticles. Results Phys 12:1230–1237
35. Baig MT, Kayan A (2024) Sol Gel obtained Ti/Co/Mn oxides doped with 5wt% CuO for the photocatalytic removal of organic azo dyes from wastewater. Mater Res Bull 180:113070
36. Demirci GV, Baig MT, Kayan A (2024) UiO-66 MOF/Zr-di-terephthalate/cellulose hybrid composite synthesized via sol-gel approach for the efficient removal of methylene blue dye. Int J Biol Macromol 283:137950
37. Maqsood K et al (2025) Synthesis and photocatalytic degradation efficiency of MgFe2O4@CuO nanocomposite for Bromophenol blue dye removal. J Chin Chem Soc 72(4):390–400
38. Maruthupandy M et al (2025) Cross-linked graphene with chitosan nanocomposites for efficient photocatalytic degradation of bromothymol blue, bromophenol blue dye molecules. Int J Biol Macromol 307:142132
39. Shahid M et al *Structural engineering of Bi2S3@MIL-100 nanocomposite for the efficient photocatalytic degradation of bromophenol blue.* Journal of the Chinese Chemical Society. n/a(n/a)
40. Fajriyansah MR et al (2025) Recyclable photocatalyst of CuFe2O4 prepared using plant extract and hydrothermal treatment for bromophenol blue degradation. Mater Lett 400:139195
41. Cong Q et al (2021) Efficient photoelectrocatalytic performance of beta-cyclodextrin/graphene composite and effect of Cl – in water: degradation for bromophenol blue as a case study. RSC Adv 11(48):29896–29905
42. Shah T, Gul T, Saeed K (2019) Photodegradation of bromophenol blue in aqueous medium using graphene nanoplates-supported TiO2. Appl Water Sci 9(4):105
43. Dlamini L et al (2011) Photodegradation of bromophenol blue with fluorinated TiO2 composite. Appl Water Sci 1(1):19–24
44. Subramaniyan R et al (2025) Sustainable method for photocatalytic dye degradation of bromophenol blue by Cu-doped ZnO nanocomposite. Chemical Papers

45. Elqahtani ZM et al (2025) Enhanced structural and optical properties of MgFe2O4 spinel ferrite by gamma irradiation for crystal violet and bromophenol blue dyes removal from wastewater. J Solgel Sci Technol 116(3):2733–2750

Figures

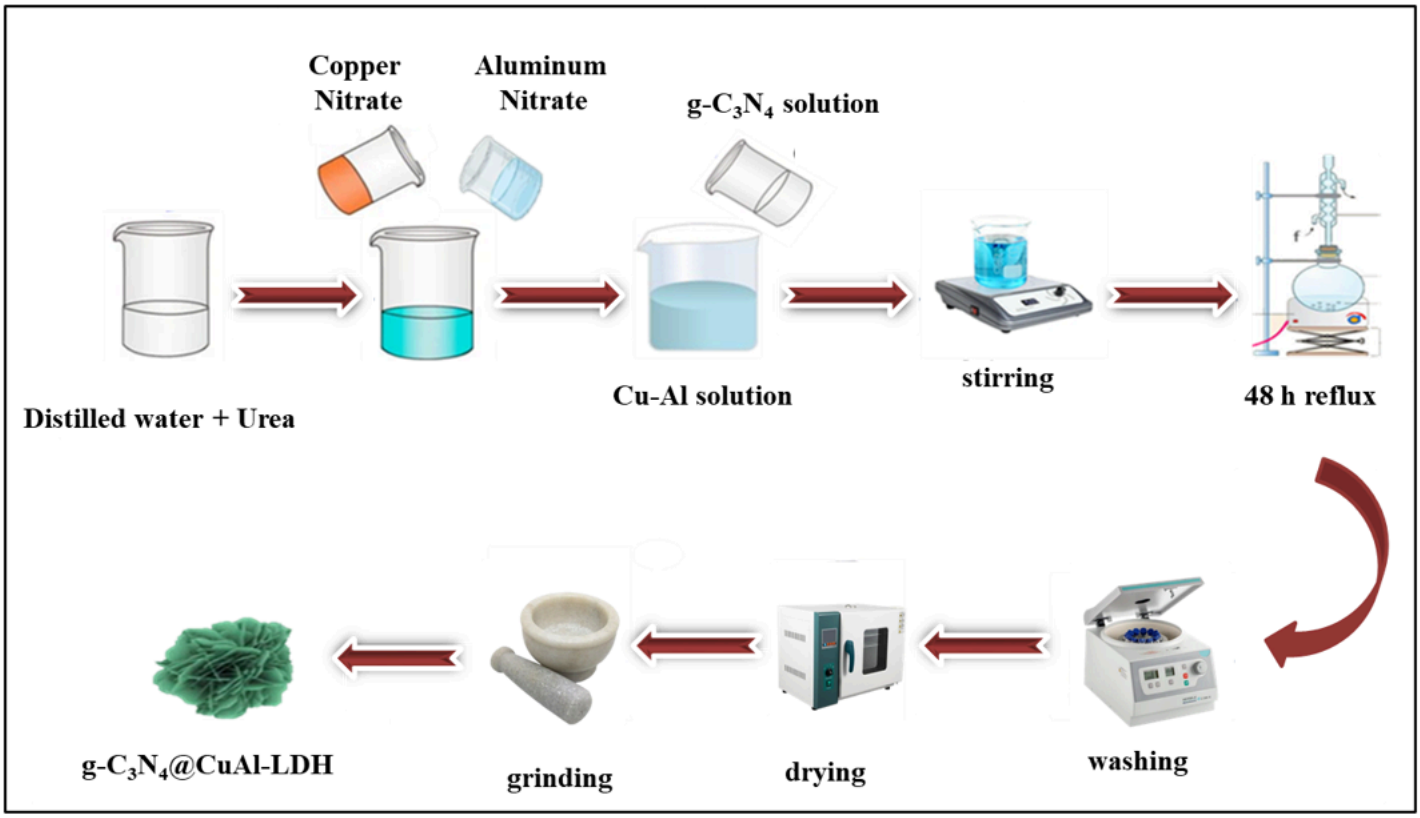

Figure 1

Schematic representation for the synthesis of g-C_3N_4@CuAl-LDH composite.

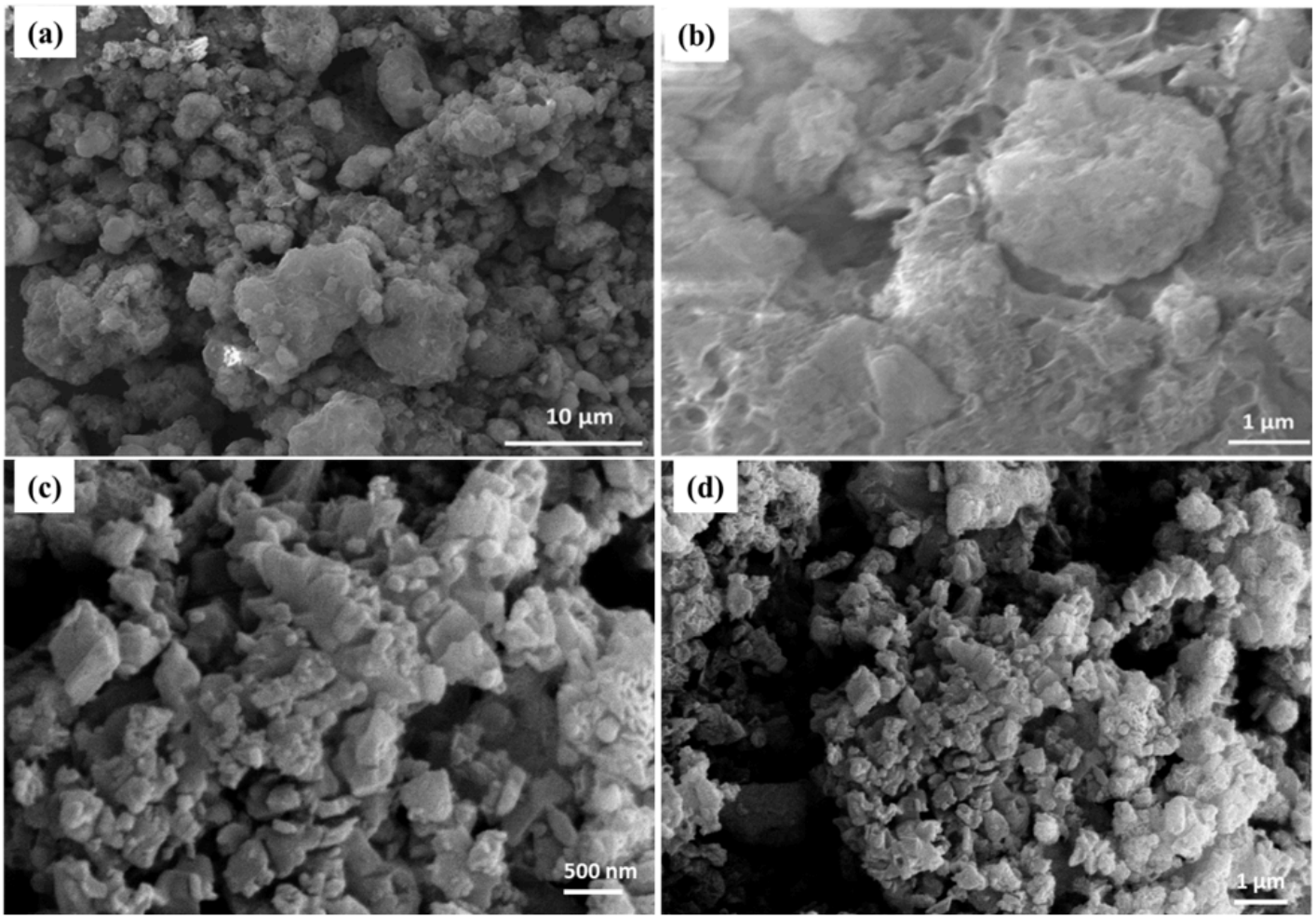

Figure 2

SEM image of (a) g-C_3N_4; (b) CuAl-LDH; (c-d) g-C_3N_4@CuAl-LDH composite

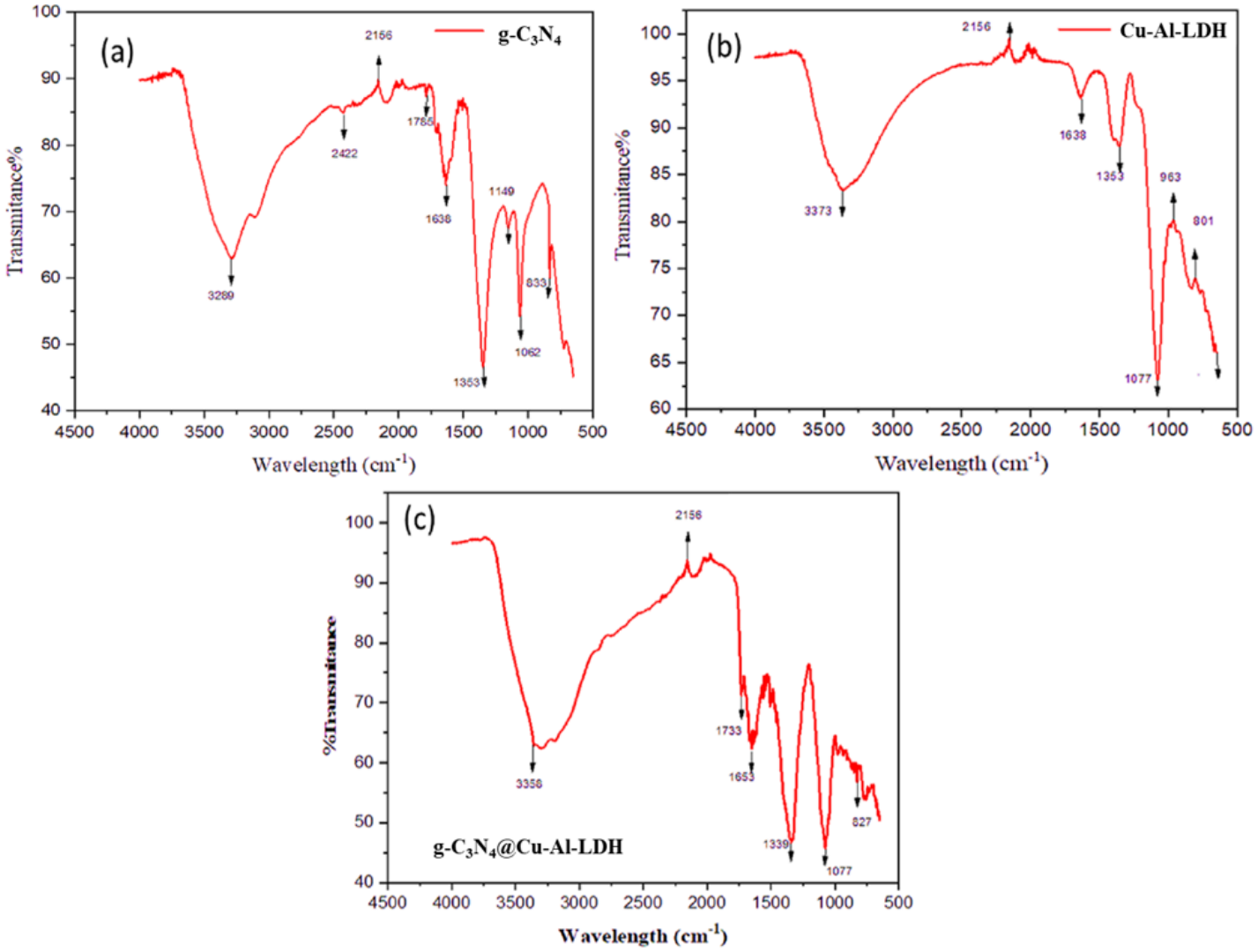

Figure 3

FTIR analysis of (a) g-C_3N_4; (b) CuAl-LDH; (c) g-C_3N_4@CuAl-LDH composite.

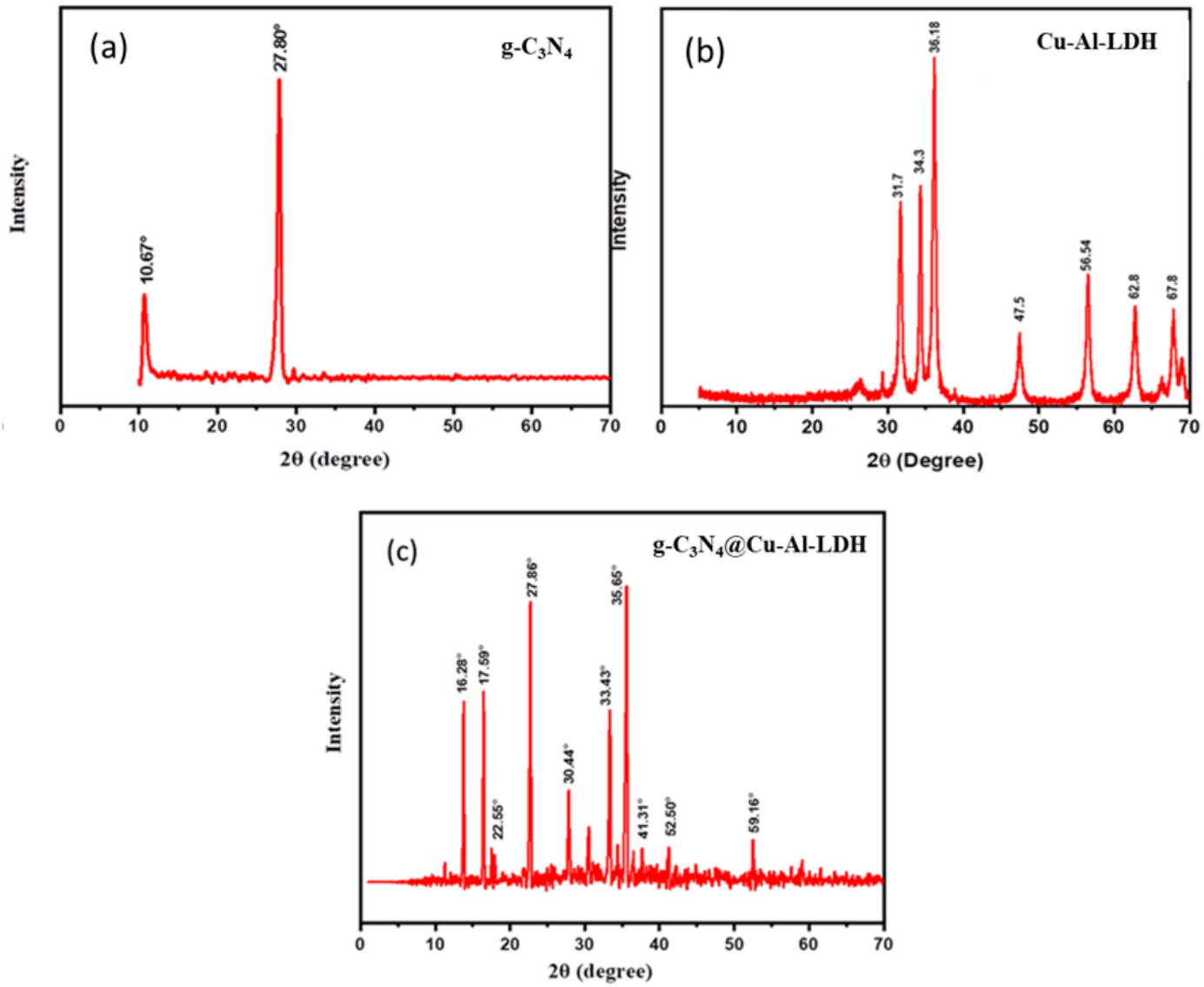

Figure 4

XRD analysis of (a) g-C_3N_4; (b) CuAl-LDH; (c) g-C_3N_4@CuAl-LDH composite.

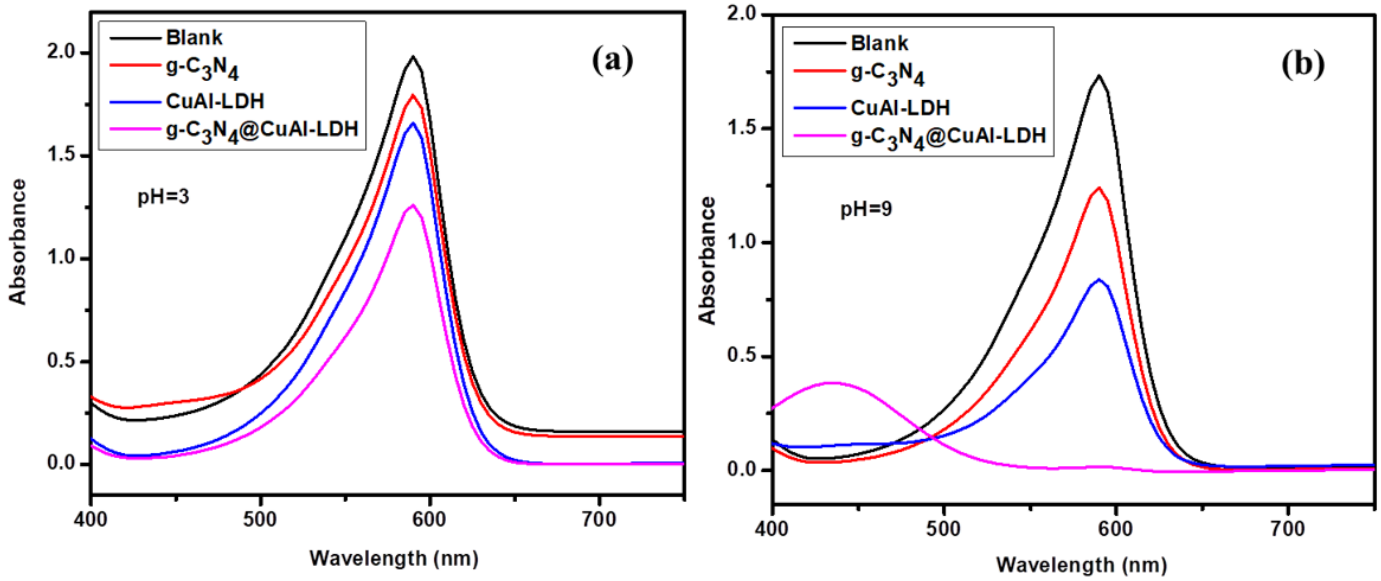

Figure 5

(a) Effect of pH 3 on the performances of as synthesized g-C_3N_4; CuAl-LDH; g-C_3N_4@CuAl-LDH; (b) Effect of pH 9 on the performances of as synthesized g-C_3N_4; CuAl-LDH; g-C_3N_4@CuAl-LDH.

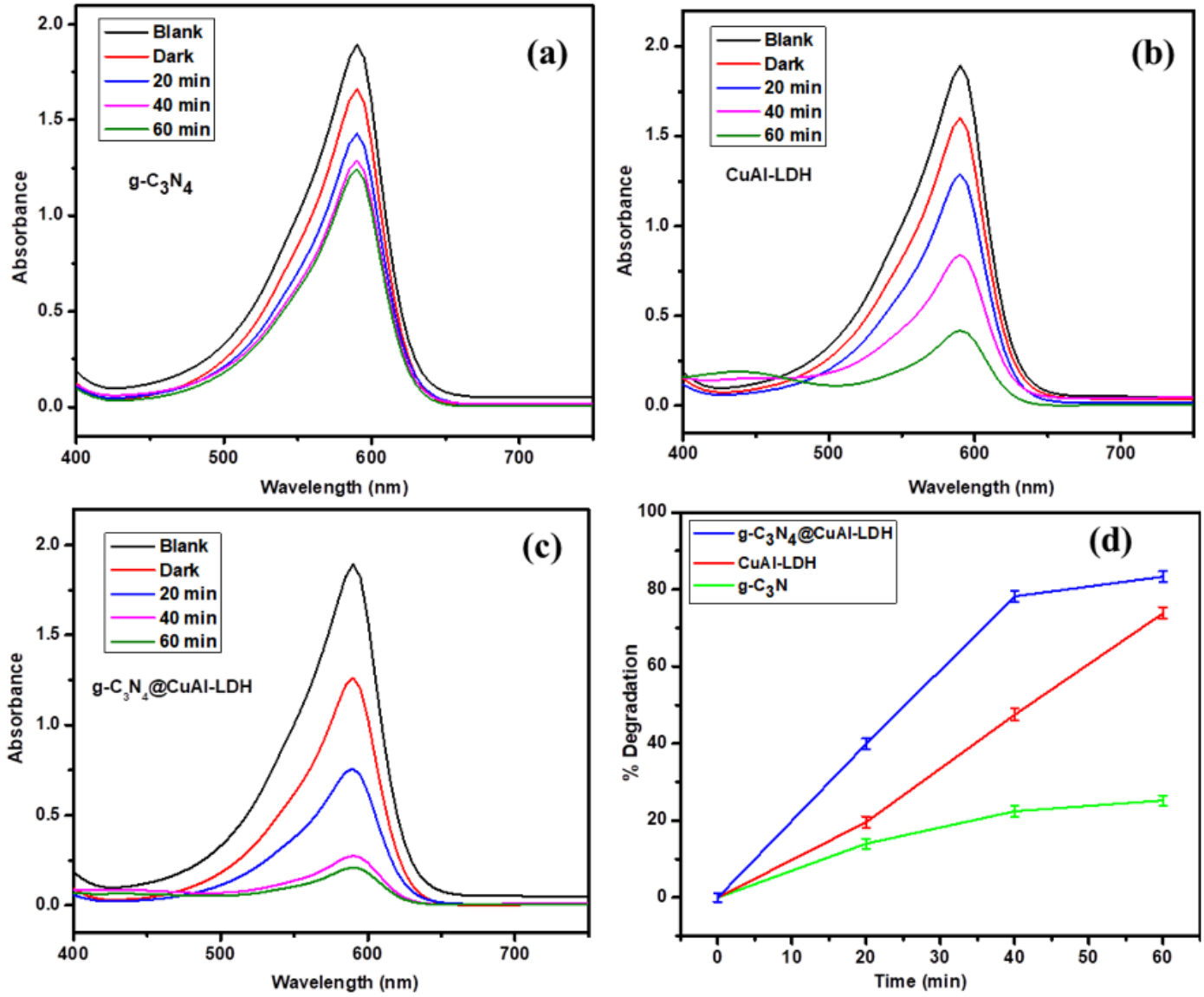

Figure 6

(a) Impact of contact time on the degradation of BPB using (a) g-C_3N_4; (b) CuAl-LDH; (c) g-C_3N_4@CuAl-LDH; (d) comparison of % degradation of as synthesized materials with respect to contact time.

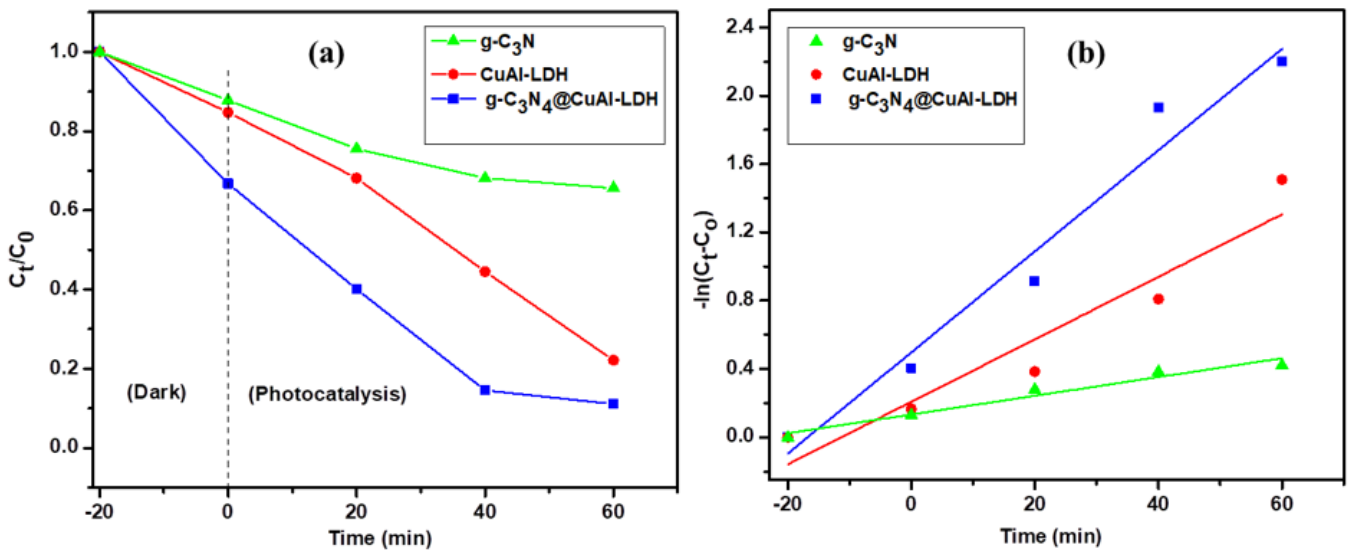

Figure 7

(a) Photocatalytic degradation of BPB under visible light using g-C_3N_4, CuAl-LDH and g-C_3N_4@CuAl-LDH; (b) Pseudo-first-order kinetics plot for g-C_3N_4, CuAl-LDH and g-C_3N_4@CuAl-LDH.

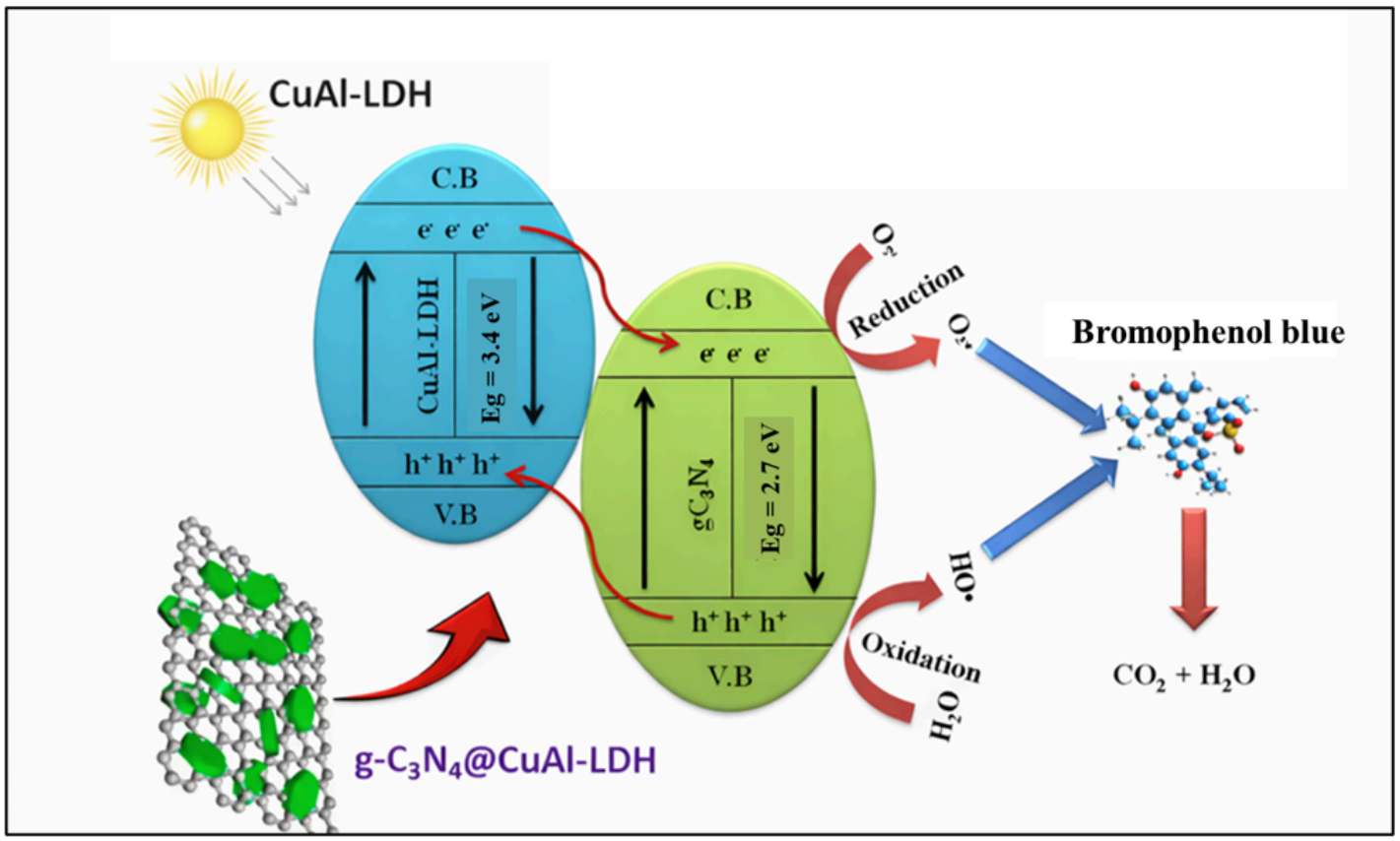

Figure 8

Proposed mechanism of photocatalytic degradation of BPB using g-C_3N_4@CuAl-LDH

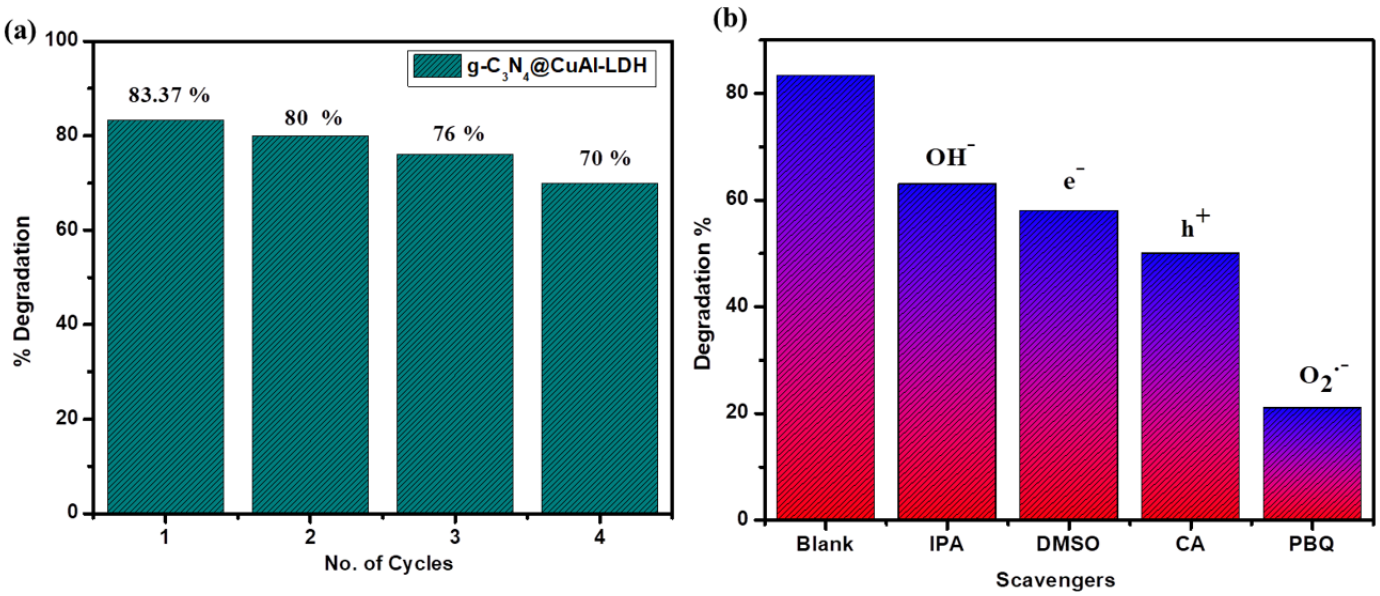

Figure 9

(a) The reusability of g-C_3N_4@CuAl-LDH composite for the degradation of BPB dye; (b) Trapping experiment for the reactive oxygen species for removal of BPB.

Supplementary Files

This is a list of supplementary files associated with this preprint. Click to download.

- floatimage1.png